Molecular dynamics investigation of dislocation pinning by a nanovoid in copper

Takahiro Hatano
Earthquake Research Institute, University of Tokyo, Tokyo 113-0032, Japan

Hideki Matsui
Institute for Materials Research, Tohoku University, Sendai 980-8577, Japan

(Received 18 February 2005; revised manuscript received 14 June 2005; published 12 September 2005)

The interaction between an edge dislocation and a void in copper is investigated by means of a molecular dynamics simulation. The depinning stresses of the leading partial and of the trailing partial show qualitatively different behaviors. The depinning stress of the trailing partial increases logarithmically with the void radius, while that of the leading partial behaves in a different manner due to the interaction between two partials. The pinning angle, which characterizes the obstacle strength, approaches zero when the void radius exceeds 3 nm. No temperature dependence is found in the critical stress and the critical angle. This is attributed to an absence of climb motion. It is also found that the distance between the void center and a glide plane asymmetrically affects the pinning strength.

DOI: 10.1103/PhysRevB.72.094105 PACS number(s): 61.80.Az, 62.20.Fe, 61.72.Qq

I. INTRODUCTION

Voids are ubiquitous in irradiated metals and act as obstacles to dislocation motion as well as other radiation-induced defects: e.g., stacking fault tetrahedra or helium bubbles. Those obstacles result in the increase of the critical stress and therefore play an important role in irradiation hardening. To investigate the extent of hardening by those obstacles, there has been a model in which a dislocation is regarded as a continuum line with the constant line tension. This is referred to as the uniform line tension model. In the presence of obstacles, a dislocation is fixed at an obstacle to form a cusp. The pinning angle ϕ is defined as the angle between two tangent vectors at a cusp. (See Fig. 1.) Then the restoring force to make a dislocation straight is written as $2\gamma\cos(\phi/2)$, where γ denotes the line tension. We assume that a dislocation can penetrate an obstacle when the restoring force exceeds the critical value. Since γ is a constant, this condition is equivalent to $\phi \leqslant \phi_c$, which we call the critical angle.

Note that stronger obstacles have smaller critical angles. A dislocation bows out to form an arc between two obstacles until the pinning angle reaches its critical value.

For a periodic array of obstacles whose spacing is L, the critical resolved shear stress (CRSS) τ_c above which a dislocation can penetrate the array of obstacles is represented by

$$\tau_c = \frac{2\gamma}{bL}\cos\frac{\phi_c}{2}, \tag{1}$$

where b denotes the Burgers vector length of a dislocation.[1] (The line tension γ is given by the elasticity theory and is often written as $Gb^2/2$, where G represents the shear modulus.)

In more realistic situations, obstacles are distributed randomly on glide planes and the randomness plays a crucial role in dislocation dynamics. In order to incorporate this effect, Foreman and Makin performed a computer simulation of the dislocation motion on a glide plane with randomly distributed obstacles of the same critical angle.[2] They found that the dislocation propagation has two qualitatively different modes depending on the critical angle. For obstacles of a small critical angle (i.e., strong obstacles), the dislocation propagation resembles dendritic growth,[3] while for a large critical angle (i.e., weak obstacles) the global form does not significantly deviate from the straight line. Also τ_c is well described by[4]

$$\tau_c = \begin{cases} \dfrac{2\gamma}{bL}\left(\cos\dfrac{\phi_c}{2}\right)^{3/2}, & \left(\phi_c \geqslant \dfrac{5}{9}\pi\right), \\ \dfrac{1.6\gamma}{bL}\cos\dfrac{\phi_c}{2}, & \left(\phi_c \leqslant \dfrac{5}{9}\pi\right), \end{cases} \tag{2}$$

where L denotes the mean spacing: the inverse of the square root of the areal density of obstacles on a glide plane.[5]

In this context, the critical angle ϕ_c, which characterizes the obstacle strength, is an important parameter to discuss the extent of hardening. However, estimation of the critical angle is not an easy task, because it involves the core structure of dislocations. In this regard, extensive molecular dynamics (MD) simulations on interactions between a dislocation and radiation-induced obstacles have been performed: e.g., stacking fault tetrahedra,[6] interstitial Frank loops,[7] voids, and copper precipitates in bcc iron.[8–10]

On the other hand, there are some experimental attempts to determine the critical angle utilizing transmission electron microscopy (TEM).[11,12] They seem to be promising but still

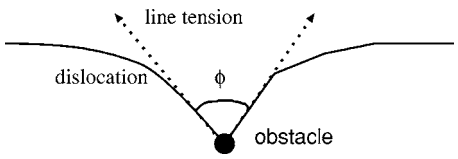

FIG. 1. A cusp formed at an obstacle. The angle ϕ between two tangential vectors is called the pinning angle.

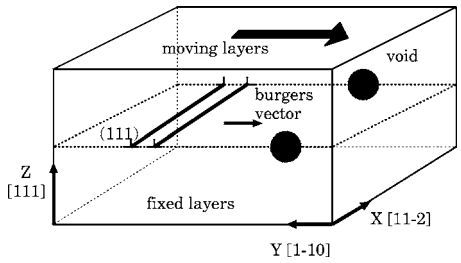

FIG. 2. Schematic of the system. Periodic boundary conditions are assigned to the x and the y directions. The system contains approximately 0.55 million atoms.

should be complemented by MD simulations in terms of the spatiotemporal resolution. For example, subnanometer obstacles cannot be seen by TEM.

In this paper, along the line of the above computational and experimental studies, we wish to estimate the critical angle and the critical stress for voids in copper. Especially, effects of the dissociation, temperature, and the distance from the void center to a glide plane are studied in detail. Note that we focus on an edge dislocation here. Results on a screw dislocation will be presented elsewhere.

This paper is organized as follows. In Sec. II, we introduce the computational model: fcc copper including an edge dislocation and a void. In Sec. III, the nature of the critical stress is investigated. Especially, the void size dependence and the temperature dependence is discussed. Section IV deals with the critical angle, which is often measured by experiments (TEM observations) to determine the obstacle strength. The discussion enables us to compare the MD simulation with the experiments. In Sec. V, the effect of the distance between the void center and a glide plane is investigated. In Sec. VI, we discuss the pinning strength of deformed voids in the context of dislocation channeling and plastic flow localization. The last section, Sec. VII, is devoted to discussions and the conclusion.

II. THE MODEL

A. The geometry

We treat fcc copper in this paper. As for the interatomic potential, we adopt the embedded-atom method of Finnis-Sinclair type[13] and choose the parameters according to Ackland *et al.*[14] The lattice constant $a=3.615$ Å.

The schematic of our system is shown in Fig. 2.

The x, y, and z axes are taken as the $[11\bar{2}]$, $[1\bar{1}0]$, and $[111]$ directions, respectively. The length of each dimension is 23, 23, and 15 nm. Periodic boundary conditions are employed in the x and the y directions. That is, dislocations of infinite length in the x direction are periodically located in the y direction.

Note that we have the surface only in the z direction, both for $z>0$ and for $z<0$. Following the procedure described in Ref. 15, three atomic layers of $[111]$ next to the lowest surface ($z<0$) are "the fixed layers" where velocities of the atoms always vanish. Similarly, three atomic layers of $[111]$ next to the upper surface ($z>0$) are "the moving layers" where velocities of the atoms are given as a constant; not given by the integration of force acting on them. The constant velocity of the moving layers causes the shear stress. Namely, the strain rate is the control parameter: not the stress. The moving layers are displaced towards the $-y$ direction: i.e., $[\bar{1}10]$.

In order to introduce a void, atoms whose barycentric positions satisfy $(x\pm L/2)^2+y^2+z^2<r^2$ are removed, where r denotes the void radius. To introduce an edge dislocation, atoms that belong to one $(1\bar{1}0)$ half plane ($z<0$) are removed and the rest of atoms are displaced by the strain field calculated from the elasticity theory. This procedure produces a perfect edge dislocation whose Burgers vector is $a/2[1\bar{1}0]$. However, a perfect dislocation in a fcc crystal is energetically unstable to split into two partial dislocations whose Burgers vector length b is $a/\sqrt{6}=1.48$ Å,

$$\frac{a}{2}[\bar{1}10] \rightarrow \frac{a}{6}[\bar{2}11]+\frac{a}{6}[\bar{1}2\bar{1}]. \tag{3}$$

Since we wish to prepare two partial dislocations and a void for the initial system, atoms are shifted by the steepest descent method in order to realize the dissociation. In addition, since our system consists of the periodic array of dislocations in the x directions due to the periodic boundary conditions, this procedure also incorporates the strain field caused by the next dislocations. After a certain relaxation time (larger than 100 ps), a perfect dislocation dissociates to yield two partial dislocations, which are separated by approximately 4 nm.

The temperature is fixed to be 300 K in this paper, except for Sec. III C where the temperature effect on the CRSS is investigated. Velocities of atoms are given by random numbers which obey the Maxwell-Boltzmann distribution. After a relatively short time required for phonon relaxation, the moving layer, which is explained above, begins to be shifted to cause the shear strain.

B. The strain rate

The strain rate $\dot{\epsilon}$ is an important parameter in dislocation dynamics. In this paper, we set $\dot{\epsilon}=8\times10^6$ (s^{-1}). Although it seems an unrealistically fast deformation, the strain rate in the MD simulation should not be directly compared with the macroscopic (or experimental) strain rate because the macroscopic strain rate involves only the average dislocation velocity. Namely, both spatial and temporal fluctuations in the dislocation velocity are neglected. The correspondence of the microscopic dislocation velocity to the macroscopic strain rate is not clear at all unless we know the statistical property of spatiotemporal fluctuations in dislocation dynamics.

Calculation of the shear stress is noteworthy. We define the shear stress as follows. Let the forces acting on the moving layers and on the fixed layers be $\mathbf{F}^{(1)}$ and $\mathbf{F}^{(2)}$, respectively. Then the shear stress τ is defined as $\tau=(|F_y^{(1)}|+|F_y^{(2)}|)/2S$, where S denotes the area of the surface and the subscript y means the y component. However, this microscopic definition of the shear stress shows a large thermal fluctuation. In addition, the inertia of the dislocation motion due to the high strain rate causes depinning at lower

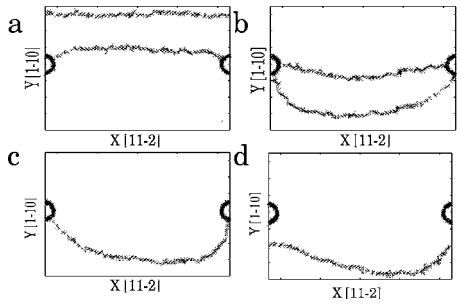

FIG. 3. Successive snapshots of a depinning process: (a) trapping of the leading partial, (b) just before the depinning of the leading partial, (c) just before depinning of the trailing partial, (d) depinning of the trailing partial. The void radius is 1 nm. To visualize the void and the dislocations, atoms that have 12 nearest neighbors are omitted. (Atoms which form dislocations have 11 or 13 nearest neighbors, and the number of nearest neighbors of void surface atoms is less than 12.)

stress.[8] In order to reduce these effects, the simulation is performed twofold. Namely, the representative point in the phase space (spanned by the positions and the momenta of all atoms) are recorded every 4.6 ps.[16] We then take the point where depinning just begins and restart the simulation with $\dot{\epsilon}=0$. In this relaxation process, the inertial effect is ruled out and the thermal fluctuation in the shear stress is averaged out. Taking this relaxation process into account, the average strain rate becomes approximately 10^6 (1/s).

III. BEHAVIORS OF THE CRITICAL RESOLVED SHEAR STRESS

A. Temporal behavior

First, we track the time evolution. Under the shear stress caused by the boundary condition, two partial dislocations glide towards the $[\bar{1}10]$ direction: the $-y$ direction. The Burgers vectors of the leading and the trailing partials are $a/6[\bar{2}11]$ and $a/6[\bar{1}2\bar{1}]$, respectively. Snapshots of a pinning-depinning process are shown in Fig. 3.

Note that there are two depinning processes corresponding to two partial dislocations, as is shown in the stress-strain relation, Fig. 4. We can see two peaks which correspond to

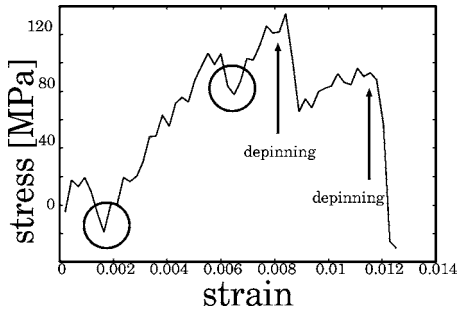

FIG. 4. Stress-strain relation. Two arrows indicate the depinning points of two partials. Two circles which indicate sudden stress drops result from the attractive interaction between the dislocations and the void.

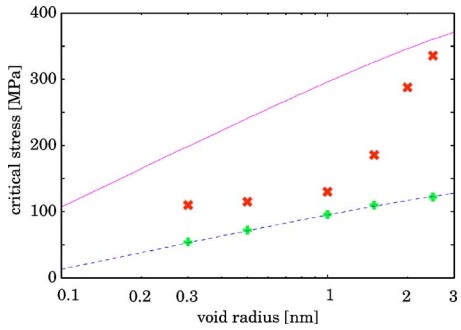

FIG. 5. (Color online) Void radius dependence of the depinning stress for the leading partial (the red symbols, ×) and for the trailing partial (the green symbols, +). The blue dashed line denotes Eq. (4) with $T=0.85$ N/m and $B=0.14$ nm. The pink dotted line denotes Eq. (6), which is the result from a continuum model calculation (Ref. 17).

each depinning process. We remark that the critical stress for the leading partial is always larger than that of the trailing partial. This is because the leading partial has already escaped from the void and keeps gliding while the trailing partial is still pinned by the void. Then the width of the stacking fault ribbon extends to cause an attractive force between the partials. Namely, depinning of the trailing partial is assisted by the attractive force from the leading partial. Also, note that the glide of the leading partial leads to the stress relaxation, which appears in the change of modulus in the stress-strain curve in Fig. 4. The modulus is 30 GPa when the leading partial is pinned ($0.002<\epsilon<0.006$), while it is 13 GPa during the depinning process of the trailing partial ($0.008<\epsilon<0.012$).

B. Void size dependence

Then the critical stress is calculated for various voids of different radii (from 0.3 to 2.5 nm). We measure the depinning stresses both for the leading partial and for the trailing partial. An interesting feature arises from the comparison of both the stresses. In Fig. 5, we can see that they have different tendencies with respect to the void radius r. The depinning stress of the trailing partial shows the well-known logarithmic dependence, while that of the leading partial undergoes a crossover around $r\simeq 1$ nm. We will discuss the difference more quantitatively in this subsection.

The depinning stress of the trailing partial can be described by the following relation:

$$\tau_c = \frac{T}{L}\log\left[\frac{2r}{B}\left(1+\frac{2r}{L}\right)^{-1}\right], \tag{4}$$

where T and B denote arbitrary constants. The best fit is realized by letting $T=0.85$ N/m and $B=0.14$ nm. Note that this logarithmic dependence has also been found in a continuum model by Scattergood and Bacon,[17] and also in the context of the Orowan mechanism.[18] As to the leading partial, the behavior of the critical stress cannot be explained in the above context. It seems to be describable by piecewise logarithmic behaviors

$$\tau_c = \begin{cases} 18 \log\left[\dfrac{2r}{1.5\times10^{-3}}\left(1+\dfrac{2r}{L}\right)^{-1}\right] \text{ MPa}, & (r \leqslant 1\text{nm}), \\ 280 \log\left[\dfrac{2r}{1.2}\left(1+\dfrac{2r}{L}\right)^{-1}\right] \text{ MPa}, & (r \geqslant 1\text{nm}). \end{cases} \tag{5}$$

Note that the extent of hardening becomes much greater when the void radius exceeds 1 nm.

Although we cannot definitely explain this phenomenon, a plausible reason lies in the interaction between two partials. When the void radius is larger than 1 nm, two partials are simultaneously trapped by the void. Then the depinning stress of the leading partial is significantly affected by a behavior of the trailing partial. As we can see in Fig. 7, the trailing partial is also bended to a certain degree as well as the leading partial. This requires excess stress, which may be responsible for the sudden increase of the critical stress for $r \geqslant 1$ nm. Meanwhile, as to $r=0.3$ and 0.5 nm, we remark that depinning of the leading partial is followed by the pinning of the trailing partial: i.e., they are not simultaneously pinned by a void. Hence, for smaller voids, the depinning of the leading partial is not affected by the trailing partial. The above explanation describes a crossover of the critical stress around $r \simeq 1$ nm. We also remark that a similar crossover due to the interaction between the dislocations is observed in the critical stress of the dislocation nucleation on the void surface.[19]

On the other hand, regardless of the void radius, the depinning of the trailing partial follows that of the leading partial. The depinning of the trailing partial is not influenced by the leading partial, since it glides far away from the void. Therefore, no crossover is seen in the critical stress. It can be described in the framework of Ref. 17, where a single dislocation involves. This is due to the absence of the interaction between the partials.

The critical stress of an edge dislocation, for which we are originally concerned, should be interpreted as the maximum stress during a pinning process. As we can see from Fig. 4, it is the depinning stress of the leading partial. Then it is interesting to compare the critical stress in the present simulation with the one obtained by Scattergood and Bacon.[17] It reads

$$\tau_{SB} = \frac{Gb}{2\pi L}\log\left[\frac{2r}{0.22b}\left(1+\frac{2r}{L}\right)^{-1}\right], \tag{6}$$

which is plotted in Fig. 5 together with the simulation result. We can see that Eq. (6) considerably overestimates the critical stress where $r \leqslant 2.5$ nm. The overestimation is attributed to the effect of dissociation, which is not taken into account in Ref. 17. Our simulation reveals the effect of dissociation in the critical stress. Nevertheless, recalling that Eq. (6) applies to a perfect edge dislocation in bcc iron,[8–10] it is plausible that the critical stress is describable by Eq. (6) for larger voids where the dissociation width is negligible compared with the void radius. Also, a continuum model in which the dissociation effect is appropriately incorporated might apply to our result. (Unfortunately, we are unaware of such an attempt at this point.)

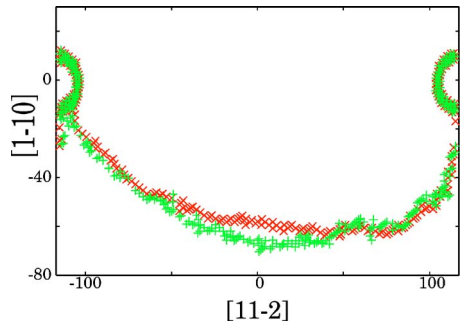

FIG. 6. (Color online) Snapshots of dislocations (the trailing partials) just before depinning. The trailing partial dislocation at 100 K is represented by × (red), and the one at 500 K is + (green). The subtle difference in the middle lies in the range of thermal fluctuation at 500 K.

C. Temperature dependence

In this section we investigate the temperature dependence of the critical stress. We calculate the critical stress for four different temperatures: 100, 200, 400, and 500 K. However, we cannot find any difference regarding the critical stress between these calculations. In Fig. 6, we show snapshots of the dislocations just before depinning, where the temperatures are 100 and 500 K, respectively. We can see no difference between the dislocation shapes. Also, the critical stress is almost the same: 130 ± 12 MPa for $r=1$ nm and 288 ± 30 MPa for $r=2.5$ nm. Namely, the temperature plays no role in the depinning processes.

Note that this result is opposite to the simulation on bcc iron with a copper precipitate.[10] There, definite temperature dependence was observed from 0 to 500 K. The reason for the difference lies in the dissociation nature of the dislocations. In bcc iron where a dislocation does not dissociate, a perfect edge dislocation absorbs vacancies from a void (or the precipitate surface) and undergoes climb motion. The extent of climb motion is remarkable for larger voids where temperature dependence of the critical stress is observed. Note that smaller voids show less temperature dependence and the climb motion is weak there. It implies that the climb motion is essential to the temperature dependence. On the other hand, no climb motion is observed in the present simulation. It is known that the climb motion is difficult in fcc crystals due to dissociation. Therefore, no temperature dependence is observed in the present simulation on fcc copper.

Another possible reason lies in the activation energy for depinning. Although the precise estimation is difficult, it is at least larger than the energy of a dislocation whose length is equivalent to the void diameter. (We neglect the step formation energy on the void surface.) The dislocation energy is calculated by the line tension multiplied by the length. The effective line tension is estimated to be 0.4 nN by Eq. (12). (Please see the next section for details.) Therefore, for the void of 2.0 nm radius, the activation energy is approximately 1.6×10^{-18} J. It is equivalent to 400 k_BT, where k_B denotes the Boltzmann constant and $T=300$ K. Since this is much larger than the thermal energy of involved atoms on the void surface (less than a hundred), it is plausible that thermal fluctuations cannot assist dislocation depinning. In addition,

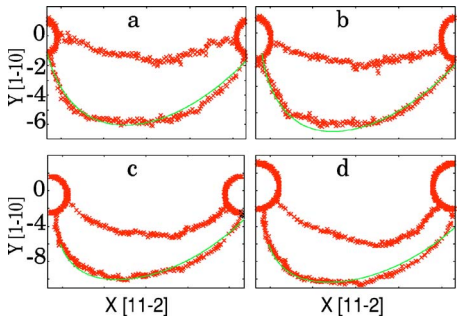

FIG. 7. (Color online) Bowing dislocations obtained by the simulation for various voids [(a) $r=1.0$ nm, (b) $r=1.5$ nm, (c) $r=2.0$ nm, (d) $r=2.5$ nm]. The green solid lines represent Eqs. (7) and (8), which are derived from an orientation dependent line tension model. Note that the trailing partials also deform to a certain degree as the void becomes larger.

please recall that the step formation energy is neglected and the actual value is larger than that. (However, in the case of precipitates, the number of involving atoms is larger than that of voids.) The above two discussions may be good reasons for the difference between fcc copper and bcc iron.

IV. THE DISLOCATION SHAPE AND THE CRITICAL ANGLE

A. An orientation dependent line tension model

As can be seen in Fig. 3, the bowing dislocation is asymmetric with respect to $x=0$. Since the uniform line tension model predicts the symmetric form (an arc), we have to incorporate an orientation dependent line tension in order to explain the asymmetric dislocation shape. Indeed, de Wit and Koehler[20] obtained a solution for the dislocation shape

$$y = C_1 + \frac{1}{\sigma b}\left[E(\theta)\cos\delta - \frac{dE}{d\theta}\sin\delta\right], \tag{7}$$

$$x = C_2 + \frac{1}{\sigma b}\left[E(\theta)\sin\delta + \frac{dE}{d\theta}\cos\delta\right], \tag{8}$$

where δ denotes the angle between the tangent line of a dislocation and the x axis. An orientation dependent line tension is denoted by $E(\theta)$, where θ represents the angle between the tangent line of the dislocation and the Burgers vector. Note that Eqs. (7) and (8) are interpreted as parametric equations with respect to δ and θ. If the concrete form of $E(\theta)$ is given, these equations can be numerically solved with an appropriate choice of the integral constants C_1 and C_2. Here, $E(\theta)$ is given as[20]

$$E(\theta) = \frac{b^2}{4\pi}\log\left(\frac{R}{r_0}\right)f(\theta), \tag{9}$$

$$f(\theta) \simeq 59.3 - 16\cos 2\theta - 0.8\cos 4\theta \ (\text{GPa}), \tag{10}$$

where r_0 is the (arbitrary) core cutoff length. In Fig. 7, Eqs. (7) and (8) are fitted with the simulation result. We can see that the fittings are quite satisfactory.

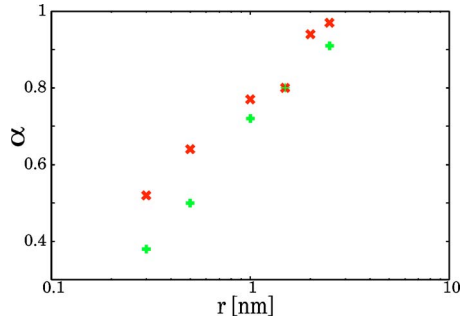

FIG. 8. (Color online) Void radius dependence of α for the leading partial (the red symbols, ×) and for the trailing partial (the green symbols, +).

B. Determination of the critical angle

In macroscopic materials, random configuration of the obstacles plays an important role in the dislocation dynamics, as was discussed in Sec. I. In order to apply Eq. (2) to practical situations, we wish to estimate the critical angle from the simulation. Note that Eq. (2) is based on the uniform line tension model, which should be regarded as the first approximation.

The critical angle ϕ_c is defined by the angle between the two tangent lines of the dislocation at the void surface. Because the critical angles are slightly different for the two partial dislocations, we measure both. The pinning strength $\alpha=\cos(\phi_c/2)$ with respect to the void radius is shown in Fig. 8.

We remark that the pinning strength α again obeys a logarithmic law

$$\alpha = A\log\frac{2r}{B\left(1+\frac{2r}{L}\right)}. \tag{11}$$

The constants are $A=0.24$ and $B=0.07$ for the leading partial, and $A=0.28$ and $B=0.15$ for the trailing partial. By extrapolation, α reaches 1 when the void radius exceeds 3 nm, as shown in Fig. 8. Note that the tendency has also been observed in the previous simulations on bcc iron.[8–10]

Meanwhile, it should be remarked that a crossover is not observed in the pinning strength α. From Eq. (1), the crossover of τ_c should be attributed to that of γ, which can be written as

$$\gamma = \frac{b\tau_c L}{2\alpha}. \tag{12}$$

Note that all of the quantities on the right-hand side of Eq. (12) are independently defined by the simulation results. The critical stress τ_c is directly computed in Sec. III, and α is the cosine of half the pinning angle, which is directly measured from the dislocation shape. The calculated line tensions are shown in Fig. 9, in which the line tension of the leading partial shows the minimum at $r=1.0$ nm while that of the trailing partial monotonically decreases. The explanation for the decrease lies in the deformations (i.e., bowouts) of the dislocations. As the void gets larger from $r=0$, the extent of

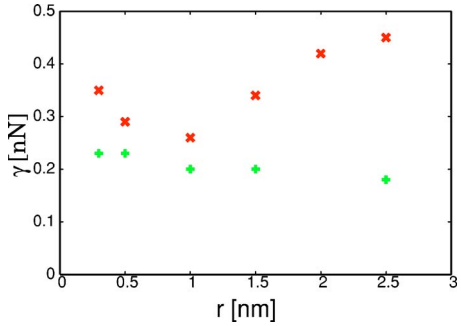

FIG. 9. (Color online) Effective line tensions estimated via Eq. (12). Those of the leading partial and of the trailing partial are represented by the red symbols (×) and the green symbols (+), respectively. Note that the void radius dependence results from the difference in the configuration of dislocations: the degree of bowing and the interactions of two partials.

the bowout becomes greater. This results in the prevalence of the screw component, since the partial dislocation is initially edgelike. The deformation lowers the effective line tension: i.e., the energy per unit length. (However, the total energy increases due to the elongation.) The above mechanism also explains the decrease of the line tension of the leading partial for $r \leqslant 1$ nm.

On the other hand, the increase of the line tension of the leading partial for $r \geqslant 1$ nm results from the interaction with the trailing partial. For larger voids, the trailing partial is also pinned by the void and bends during the depinning process of the leading partial, as can be seen in Fig. 7. That effectively increases the line tension of the leading partial.

V. EFFECTS OF THE IMPACT PARAMETER

So far, we have limited ourselves to the situation where a dislocation penetrates the void center. This is rather a special case, because the relative position of a void to a glide plane is arbitrary. In this section, we change the distance between the void center and a glide plane. We call the distance "the impact parameter," which is denoted by d. (See Fig. 10.)

The pinning strength α is estimated for the various impact parameters. The result is shown in Fig. 11, which shows asymmetric dependence of α on d. Note that a dislocation is pinned even when it is not in contact with a void. It implies that, as well as the core energy, the elastic strain around a

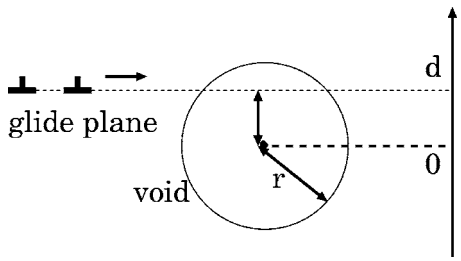

FIG. 10. The impact parameter d is defined by the distance from the void center to the glide plane. Note that the lower part of the void corresponds to the negative values of d.

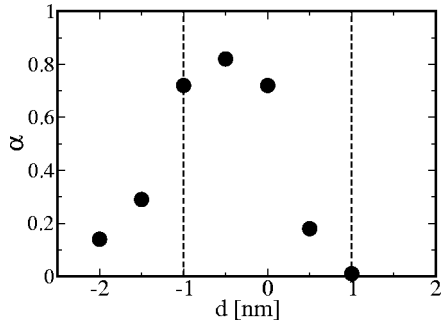

FIG. 11. Impact parameter dependence of the pinning strength α for the trailing partial. Void radius is 1.0 nm (indicated by the dashed lines).

dislocation plays an important role in the pinning phenomena. In addition, the asymmetry regarding $d=0$ comes from the nature of the strain field around an edge dislocation: i.e., the existence of hydrostatic pressure caused by an extra atomic plane. Especially, the fact that the pinning strength becomes considerably weak for $d>0$ suggests that the hydrostatic pressure is dominant over the shear stress.

Also, we remark that strong pinning ($\alpha \geqslant 0.5$) occurs only where $-1.0r \leqslant d \leqslant 0$: i.e., the lower half of the void. This area accounts for approximately 30% or 40% of the whole pinning region, while the rest involves relatively weak pinning. The large variance of the pinning strength distribution for a single void suggests reconsideration of the same pinning strength assumption in dislocation dynamics simulations. In Sec. VII, we discuss how to incorporate this effect into the estimation of the critical stress in the framework of Eq. (2).

VI. EFFECTS OF VOID DEFORMATION AFTER THE PASSAGE OF SEVERAL DISLOCATIONS

When a void is sheared by a dislocation, two parts which are divided by the glide plane are displaced to each other by the Burgers vector. After the passages of several dislocations, it may collapse and lose the pinning ability. For example, the collapse of the stacking fault tetrahedra by the passage of dislocations is both experimentally[22] and computationally[6] observed. This phenomenon is believed to be responsible for the formation of the dislocation channel and the localization of plastic flow, which recently invokes attention including some computational studies.[21] In this section, the effect of the void deformation on the pinning strength is discussed based on the motivation described above.

We remark that another possible mechanism of the void deformation is vacancy absorption by (and the climb motion of) an edge dislocation, as was discussed in Sec. III C. However, no climb motion was seen in our simulations, because the climb is difficult in fcc metals due to dissociation. Hence, we do not consider the void contraction by the climb of dislocations. We concentrate on the effect of the relative deformation with respect to a glide plane.

We prepare the deformed void as shown in Fig. 12. First we prepare a spherical void. Then, instead of iterating the pinning simulations, atoms located above the glide plane are

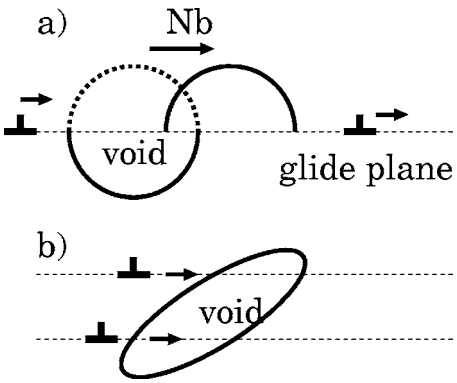

FIG. 12. Schematic of the void deformation by the passages of N edge dislocations. (a) There is a single glide plane which cuts the void center. (b) Glide planes are uniformly distributed. Each plane has N dislocations which penetrate the void.

displaced by the Burgers vector $a/2[\bar{1}10]$. Iterating this procedure for N times is equivalent to the passage of N edge dislocations.

We set two configurations. In case (a), a glide plane on which a dislocation moves is assumed to be at the void center, whereas glide planes are uniformly distributed in case (b).

In case (a), we set $N=5$ and $N=10$. Namely, a void is assumed to be penetrated by the dislocations on the same glide plane five times or ten times. The pinning strength α is found to be 0.7 for both cases, which is almost the same value as the one for the spherical void. This is consistent with the result obtained in the last section that the upper part of the void is dominant in the pinning of the edge dislocations because of the hydrostatic pressure. In case (b), we test $N=2$ and cannot find any difference from the nondeformed case regarding the critical angle. Thus, as far as the vacancy absorption mechanism (i.e., climb) is absent, the pinning strength is not seriously altered by the passage of dislocations.

VII. DISCUSSIONS AND CONCLUDING REMARKS

A. Practical applications

Let us estimate the critical stress of copper in which voids are randomly distributed. First, we determine the average spacing L between obstacles on a glide plane. The areal density is represented as $2r\rho$, where ρ denotes the number density of voids per unit volume. Then the average spacing on a glide plane is written as $L=1/\sqrt{2r\rho}$. Since the expression includes all the voids which intersect a glide plane, their impact parameters are randomly distributed from $-r$ to r. Since we have seen that the pinning strength α considerably changes with the impact parameter d in Sec. V, we wish to incorporate this result. However, at this point, there is no simulation which considers this effect. Therefore, we have to resort a rough approximation here. From Fig. 11, strong pinning ($\alpha \geqslant 0.4$) occurs only where $-1.2r \leqslant d \leqslant 0.2r$. We neglect the rest. Namely, it is assumed that only this region is responsible for pinning. We use $1.4r$ instead of the diameter $2r$; then $L \simeq 1/\sqrt{1.4r\rho}$. We can rewrite Eq. (2) as

$$\tau_c = \frac{1.6\gamma\alpha}{b}\sqrt{1.4r\rho}, \tag{13}$$

where the line tension γ should be interpreted as the effective one that is determined by the present simulation, Fig. 9.

For example, an irradiated copper specimen includes voids whose average diameter $2r=4.1$ nm, and the number density ρ is 2.9×10^{22} m^{-3}.[23] From the present simulation, the line tension γ and the pinning strength α are estimated as 0.42 nN and 0.9, respectively. The effective areal density is then calculated as 8.4×10^{-5} nm^{-2} (i.e., the average spacing is 110 nm). This yields $\tau_c=21$ MPa, which is a reasonable value. In order to give more precise predictions, Eq. (2) should be modified to include the effect of the impact parameter and an orientation dependent line tension.

B. Comparison with a continuum model with self-interaction

Scattergood *et al.* have presented a model calculation on the dislocation pinning by a void, based on the framework of Bacon *et al.*[18] It is a continuum model that incorporates the self-interaction of a dislocation. Since their system also consists of the periodic array of voids, we wish to compare their result to ours.

Let us briefly review their discussion. They have speculated that dislocation pinning concerns the line tension near the pinning point. Since a dislocation rotates by almost $\pi/2$ there, we regard the effective line tension as that of its counterpart. For example, as for an edge dislocation, the effective line tension near the void surface is that of a screw dislocation. Then the depinning stress for an edge dislocation is expressed by

$$\tau = \frac{2\gamma_{\mathrm{eff}}}{Lb}, \tag{14}$$

$$\gamma_{\mathrm{eff}} = \frac{Gb^2}{4\pi}\log\bar{R}, \tag{15}$$

$$\frac{1}{\bar{R}} = \frac{B}{L-2r} + \frac{B}{2r}, \tag{16}$$

where $\bar{R}$ should be interpreted as the effective outer cutoff divided by the core cutoff. Note that B itself is not the core cutoff but an unknown function of the core cutoff. The above equations yield Eq. (6).

Their discussion can be extended to a dislocation of arbitrary orientation

$$\gamma_{\mathrm{eff}} = \frac{Gb^2}{4\pi(1-\nu)}\left[1-\nu\cos^2\left(\frac{\pi}{2}-\theta\right)\right]\log\bar{R}, \tag{17}$$

where ν and θ denote Poisson's ratio and the angle between the dislocation line and the Burgers vector, respectively. In the present case, substituting $\theta=\pi/3$ (for the partials) into Eq. (17) yields $\tau=30\log\bar{R}$ MPa. Recall that Eq. (17) is an expression for the resolved shear stress with respect to the

Burgers vector of a partial dislocation. It is equivalent to $\tau = 35 \log \bar{R}$ MPa with respect to the Burgers vector of an original perfect dislocation. Indeed, it shows an excellent agreement with the critical stress of the trailing partial. Therefore, we confirm that the extended form of the effective line tension, Eq. (17), agrees with the present simulation, if there is no strong interaction between the partials. Note that the arbitrary parameter B is inevitable as long as continuum models for dislocations are involved.

C. Conclusion

We calculated the critical stress and the critical pinning angle for the interaction between an edge dislocation and a void in fcc copper. Dissociation of a dislocation plays an important role in the behaviors of the critical stress: (i) It is much lower than the estimation of Scattergood and Bacon, which does not consider dissociation. (ii) It suddenly increases at a certain void radius where two partials are simultaneously trapped. (iii) The depinning stress of the trailing partial does agree with that of Scattergood and Bacon, since the leading partial moves far from the void.

We also found that there is no temperature dependence in the critical stress and the pinning angle. This is opposite to the previous simulation on bcc iron.[8–10] The difference comes from the presence (bcc) or the absence (fcc) of the climb motion.

The pinning strength $\cos(\phi_c/2)$ obeys the empirical logarithmic law which has been found in Refs. 17 and 18. The distance between the void center and the glide plane (the impact parameter) is found to affect the pinning strength in asymmetric manner. This is due to the hydrostatic pressure around an edge dislocation. Hence, it is interesting to compare the result with that of a screw dislocation, which is a work in progress.

The impact parameter dependence of the critical angle also suggests the importance of randomness in the pinning strength. Even if a system contains voids of the same radius, the cross section on a glide plane is randomly distributed. Hence, we have to incorporate the randomness in the pinning strength. It is not straightforward to deduce this effect from the existing simulations which treat only two kinds of obstacles.[24] The investigation of a continuum model with random pinning angles will be interesting to see how the impact parameter dependence affects the macroscopic dislocation motion.

ACKNOWLEDGMENTS

The authors gratefully acknowledge Nobuyasu Nita for useful discussions regarding experimental situations. They also thank Yuhki Satoh and Hideo Kaburaki for discussions and valuable comments.

[1] K. C. Russel and L. M. Brown, Acta Metall. **20**, 969 (1972).
[2] A. J. E. Foreman and M. J. Makin, Philos. Mag. **14**, 911 (1966).
[3] The existence of the two modes in one-dimensional surface propagation was rediscovered by Cieplak and Robbins in the context of fluid invasion in porous media. M. Cieplak and M. O. Robbins, Phys. Rev. B **41**, 11508 (1990); Phys. Rev. Lett. **60**, 2042 (1988).
[4] The validity of the definition of critical resolved shear stress in the dendritic-growth mode is questionable because of the considerable inhomogeneity of plastic flow. In addition, the self-interaction can no longer be negligible there.
[5] U. F. Kocks, Can. J. Phys. **45**, 737 (1967).
[6] B. D. Wirth, V. V. Bulatov, and T. Diaz de la Rubia, J. Eng. Mater. Technol. **124**, 329 (2002).
[7] D. Rodney and G. Martin, Phys. Rev. Lett. **82**, 3272 (1999); D. Rodney, Acta Mater. **52**, 607 (2004).
[8] Yu. N. Osetsky and D. J. Bacon, J. Nucl. Mater. **323**, 268 (2003).
[9] Yu. N. Osetsky, D. J. Bacon, and V. Mohles, Philos. Mag. **83**, 3623 (2003).
[10] D. J. Bacon and Yu. N. Osetsky, J. Nucl. Mater. **329-333**, 1233 (2004).
[11] J. S. Robach, I. M. Robertson, B. D. Wirth, and A Arsenlis, Philos. Mag. **83**, 955 (2003).
[12] K. Nogiwa, T. Yamamoto, K. Fukumoto, H. Matsui, Y. Nagai, K. Yubuta and M. Hasegawa, J. Nucl. Mater. **307-311**, 946 (2002).
[13] M. W. Finnis and J. E. Sinclair, Philos. Mag. A **50**, 45 (1984).
[14] G. J. Ackland, D. J. Bacon, A. F. Calder, and T. Harry, Philos. Mag. A **75**, 713 (1997).
[15] Yu. N. Osetsky and D. J. Bacon, Modell. Simul. Mater. Sci. Eng. **11**, 427 (2003).
[16] For the strain rate adopted here (8×10^6 1/s), the duration between the snapshots (4.6 ps) corresponds to the strain of 3.68×10^{-5}. Multiplying the shear modulus, it approximately corresponds to 1.8 MPa. Therefore, we have uncertainty of 1.8 MPa in determining the critical stress due to the discreteness. But we believe the errors of this order do not matter.
[17] R. O. Scattergood and D. J. Bacon, Acta Metall. **30**, 1665 (1982).
[18] D. J. Bacon, U. F. Kocks, and R. O. Scattergood, Philos. Mag. **28**, 1241 (1973).
[19] T. Hatano, Phys. Rev. Lett. **93**, 085501 (2004).
[20] G. de Wit and J. S. Koehler, Phys. Rev. **116**, 1113 (1959).
[21] T. D. de la Rubia, H. M. Zbib, T. A. Khraishi, B. D. Wirth, M. Victoria, and M. J. Caturla, Nature **406**, 871 (2000).
[22] Y. Matsukawa and S. J. Zinkle, J. Nucl. Mater. **329-333**, 919 (2004).
[23] N. Nita (unpublished).
[24] A. J. E. Foreman and M. J. Makin, Can. J. Phys. **45**, 511 (1967).